PITX2 upregulation increases the risk of chronic atrial fibrillation in a dose-dependent manner by modulating I_{Ks} and I_{CaL}—insights from human atrial modelling

Jieyun Bai[1], Yaosheng Lu[1], Andy Lo[2], Jichao Zhao[2], Henggui Zhang[3]

[1]Department of Electronic Engineering, College of Information Science and Technology, Jinan University, Guangzhou 510632, China; [2]Auckland Bioengineering Institute, The University of Auckland, Auckland, New Zealand; [3]Biological Physics Group, School of Physics & Astronomy, University of Manchester, Manchester, UK

Contributions: (I) Conception and design: J Bai, J Zhao, H Zhang; (II) Administrative support: Y Lu; (III) Provision of study materials or patients: J Zhao; (IV) Collection and assembly of data: J Bai; (V) Data analysis and interpretation: J Bai; (VI) Manuscript writing: All authors; (VII) Final approval of manuscript: All authors.

Correspondence to: Jieyun Bai. Department of Electronic Engineering, College of Information Science and Technology, Jinan University, Guangzhou 510632, China. Email: baijieyun@jnu.edu.cn; Jichao Zhao. Auckland Bioengineering Institute, The University of Auckland, Auckland 1010, New Zealand. Email: j.zhao@auckland.ac.nz; Henggui Zhang. Biological Physics Group, School of Physics & Astronomy, University of Manchester, Manchester M13 9PL, UK. Email henggui.zhang@manchester.ac.uk.

Background: Functional analysis has shown that the paired-like homeodomain transcription factor 2 (PITX2) overexpression associated with atrial fibrillation (AF) leads to the slow delayed rectifier K^+ current (I_{Ks}) increase and the L-type Ca^{2+} current (I_{CaL}) reduction observed in isolated right atrial myocytes from chronic AF (CAF) patients. Through multiscale computational models, this study aimed to investigate the functional impact of the PITX2 overexpression on atrial electrical activity.

Methods: The well-known Courtemanche-Ramirez-Nattel (CRN) model of human atrial action potentials (APs) was updated to incorporate experimental data on alterations in I_{Ks} and I_{CaL} due to the PITX2 overexpression. These cell models for sinus rhythm (SR) and CAF were then incorporated into homogeneous multicellular one-dimensional (1D), two-dimensional (2D), and three-dimensional (3D) tissue models. The proarrhythmic effects of the PITX2 overexpression were quantified with ion current profiles, AP morphology, AP duration (APD) restitution, conduction velocity restitution (CVR), wavelength (WL), vulnerable window (VW) for unidirectional conduction block, and minimal substrate size required to induce re-entry. Dynamic behaviors of spiral waves were characterized by measuring lifespan (LS), tip patterns and dominant frequencies.

Results: The I_{Ks} increase and the I_{CaL} decrease arising from the PITX2 overexpression abbreviated APD and flattened APD restitution (APDR) curves in single cells. It reduced WL and increased CV at high excitation rates at the 1D tissue level. Although it had no effects on VW for initiating spiral waves, it decreased the minimal substrate size necessary to sustain re-entry. It also stabilized and accelerated spiral waves in 2D and 3D tissue models.

Conclusions: Electrical remodeling (I_{Ks} and I_{CaL}) due to the PITX2 overexpression increases susceptibility to AF due to increased tissue vulnerability, abbreviated APD, shortened WL and altered CV, which, in combination, facilitate initiation and maintenance of spiral waves.

Keywords: Atrial fibrillation (AF); paired-like homeodomain transcription factor 2 (PITX2); modelling and simulation; human atrial action potential model (human atrial AP model); electrical and structural remodeling

Submitted Oct 15, 2019. Accepted for publication Dec 24, 2019.
doi: 10.21037/atm.2020.01.90
View this article at: http://dx.doi.org/10.21037/atm.2020.01.90

Introduction

Atrial fibrillation (AF) is the most common sustained heart rhythm disorder resulting in substantial burden in terms of costs and morbidity (1). AF has a high rate of adverse events including stroke, gastrointestinal hemorrhage and heart failure (2). Characterized by rapid and irregular atrial electrical activation, AF is associated with sustained reentrant rotors (3,4) and ectopic activity (5-7). Although actionable patient-specific AF mechanisms are as yet incompletely understood, electrical remodeling of ion channels (8-10) and structural abnormalities (i.e., alterations of atrial muscle, the cavity and connective tissue) (11) are major dynamic factors needed for the initiation, progression, and maintenance of AF. However, genome-wide association studies suggested genetic variation contributes to AF susceptibility, with >100 AF-associated loci reported to date (12-15), including the atrial-selective transcription factor paired-like homeodomain transcription factor 2 (PITX2) (16-18).

The single nucleotide polymorphisms associated with AF are located in a noncoding region of human chromosome 4q25, ~170 kb distal to the PITX2 gene (19-23). PITX2 plays a critical role in generating and maintaining morphologic and electrical cardiac asymmetry (24-26). In AF patients, alterations in PITX2 expression can lead to abnormalities in atrial electrical properties (27-30), suggesting the key role of PITX2 in the pathophysiology of AF. Understanding the pro-arrhythmic role of electrical remodeling induced by PITX2 is an essential step to understand and treat AF.

Recently, Pérez-Hernández *et al.* for the first time measured the PITX2 expression in human right atrial myocytes from sinus rhythm (SR) and chronic AF (CAF) patients and investigated the effects of PITX2 on the slow delayed rectifier K^+ current (I_{Ks}) and the L-type Ca^{2+} current (I_{CaL}) (16). In this study, polymerase chain reaction analysis showed that PITX2 mRNA expression was increased in AF myocytes. PITX2 increased transcriptional activity of KCNQ1 and KCNE1 genes (the I_{Ks} channel β-subunit), whereas it inhibited I_{CaL} via post-translational modifications. Interestingly, the increase of PITX2 expression correlated with the I_{Ks} increase and I_{CaL} reduction, which characterized PITX2-induced electrical remodeling.

Electrical remodeling due to PITX2 alterations is likely to manifest as modifications to action potential (AP) morphology and AP duration (APD). In a previous simulation study, it has been shown that changes in electrical properties (I_{Na}, I_{CaL}, I_{Ks}, I_{K1} and calcium handling) resulted from PITX2 insufficiency in the adult left atrium abbreviates human atrial AP (31), indicating AF susceptibility. By contrast, whilst alterations in ion channels (I_{Ks} and I_{CaL}) due to PITX2 overexpression in the human right atrium have been suggested to enhance AF recurrence and maintenance (16), the link remains to be demonstrated directly. Since complex electrical wave dynamics observed during AF is determined by AP morphology, APD, conduction velocity restitution (CVR), wavelength (WL), vulnerable window (VW) for unidirectional conduction block, and minimal substrate size required to induce re-entry (32-34), the mechanisms by which altered I_{Ks} and I_{CaL} induced by the PITX2 overexpression promote and perpetuate AF have not yet been elucidated. Therefore, utilizing a multi-scale computational model of the human atria based on experimental data on PITX2-induced electrical remodeling, this study was to quantify the functional impact of the PITX2 overexpression on the electrical activity at the cellular, one-dimensional (1D) fiber tissue, two-dimensional (2D) sheet tissue and three-dimensional (3D) atria levels.

Methods

Simulations were based on the Courtemanche-Ramirez-Nattel (CRN) model for human atrial cardiomyocyte (35). The model was chosen in the present study because it is well suited to the study of re-entrant arrhythmias (8,36). The model was modified to incorporate the experimental data of Pérez-Hernández *et al.* on the changes in I_{Ks} and I_{CaL} due to the PITX2 overexpression (16).

To obtain the model parameters that reproduced the experimentally-observed kinetic properties of SR and AF currents, we simulated the experimental current-voltage (I-V) relationships using the voltage clamp protocol from Pérez-Hernández *et al.* (16). Equations and parameters for I_{Ks} are given by:

$$g_{ks} = 0.129\ mS/\mu F \quad [1]$$

$$xs_{\infty} = \frac{1}{\sqrt{1+\exp\left(\frac{19.9-V}{12.7}\right)}} \quad [2]$$

$$Tau_{xs} = \frac{0.5}{0.00004\cdot\frac{(V-19.9)}{1-\exp\left(\frac{19.9-V}{17}\right)}+0.000035\cdot\frac{(V-19.9)}{1-\exp\left(\frac{V-19.9}{9}-1\right)}} \quad [3]$$

$$I_{KS,SR} = g_{Ks}\cdot xs\cdot xs\cdot(V-E_{Ks}) \quad [4]$$

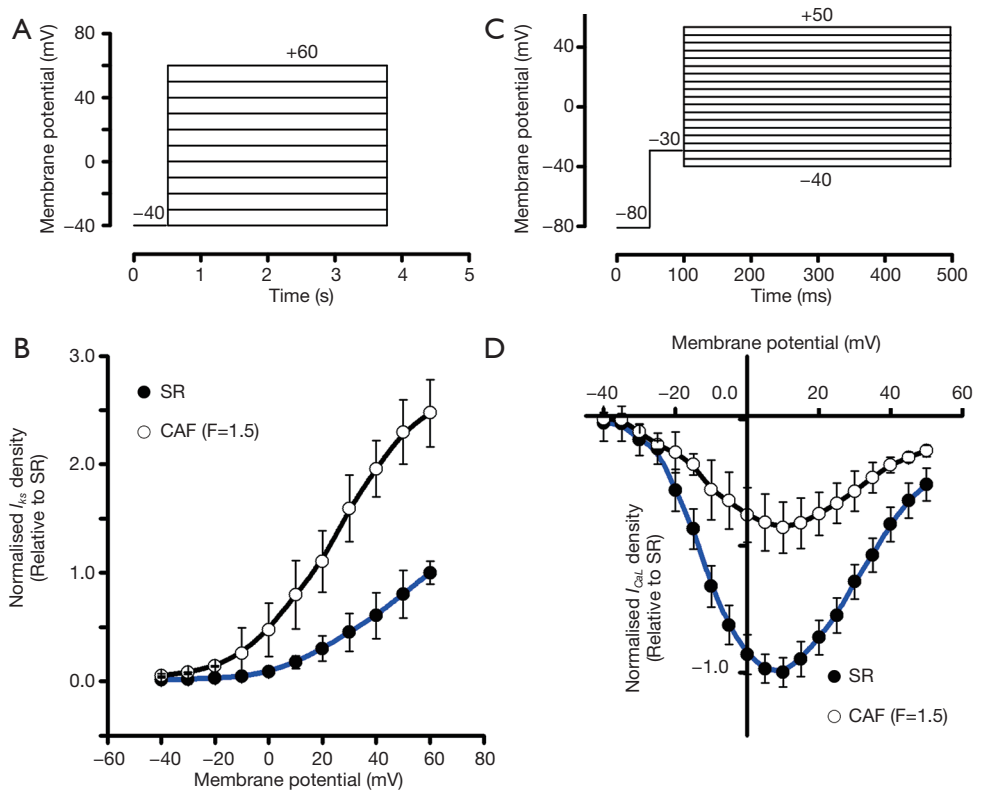

Figure 1 I_{Ks} and I_{CaL} under SR and CAF conditions, where the expression level of PITX2 under the CAF (F=1.5) condition is 1.5-fold more than that under the SR condition. Voltage-clamp protocol (A) and I-V relationships (B) for SR I_{Ks} (filled circles) and CAF I_{Ks} (open circles); the protocol (C) applied for obtaining current density-voltage curves (D) for SR and CAF I_{CaL} cases. SR, sinus rhythm; CAF, chronic atrial fibrillation; PITX2, paired-like homeodomain transcription factor 2; I_{Ks}, the slow delayed rectifier K^+ current; I_{CaL}, the L-type Ca^{2+} current; I-V, current-voltage.

$$I_{KS,AF} = I_{KS,SR} + 1.2 \cdot F \cdot g_{KS} \cdot xs \cdot (V + 75.3) \quad [5]$$

where g_{KS} is the maximal conductance, xs_∞ and Tau_{xs} denote for the steady-state for activation and the time constant for xs_∞, respectively. V is voltage, E_{KS} is the equilibrium (Nernst) potential, and xs is an activation gate. $I_{KS,SR}$ and $I_{KS,AF}$ denote the I_{KS} potassium current under SR and AF conditions, respectively. F is a scaling factor between 0 (SR) and 1.5 (AF) enabling simulation of possible intermediate conditions (F changes from 0 to 1.5).

Equations and parameters for I_{CaL} are given by:

$$g_{ICaL} = 0.1238\, mS/\mu F \quad [6]$$

$$I_{ICaL,SR} = g_{ICaL} \cdot d \cdot f \cdot f_{Ca} \cdot (V - E_{CaL}) \quad [7]$$

$$I_{ICaL,AF} = (1 - 0.35 \cdot F) \cdot I_{ICaL,SR} \quad [8]$$

where g_{ICaL} is the maximal conductance, E_{CaL} (65.0 mV) is the Ca^{2+} reversal potential, and d, f and f_{Ca} are gate variables. $I_{ICaL,SR}$ and $I_{ICaL,AF}$ denote the I_{ICaL} calcium current under SR and AF conditions, respectively. The steady state properties of these gates are described in the original CRN model (35).

Using the protocol shown in *Figure 1A*, I-V relationships of I_{Ks} for the SR and the CAF (F=1.5) conditions are present in *Figure 1B*. Confirming experimental results of Pérez-Hernández *et al.* (16), in the CAF (F=1.5) model, I_{Ks} density increased ~2-fold (at +60 mV) compared with the SR model. Based on the voltage clamp protocol for I_{CaL} (*Figure 1C*), I-V curves of I_{CaL} were compared between the SR and CAF (F=1.5) conditions (*Figure 1D*). I_{CaL} density at +10 mV under the CAF (F=1.5) condition was smaller than that in the SR case. These main changes of I_{Ks} and I_{CaL} were consistent with observations in the previous study of Pérez-Hernández *et al.* (16) In the following simulations, the intermediate states (F=0.5 and 1.0) between SR and CAF (F=1.5) were also investigated.

Details were provided in the Supplementary file 1 regarding multiscale models of human atria, which consist

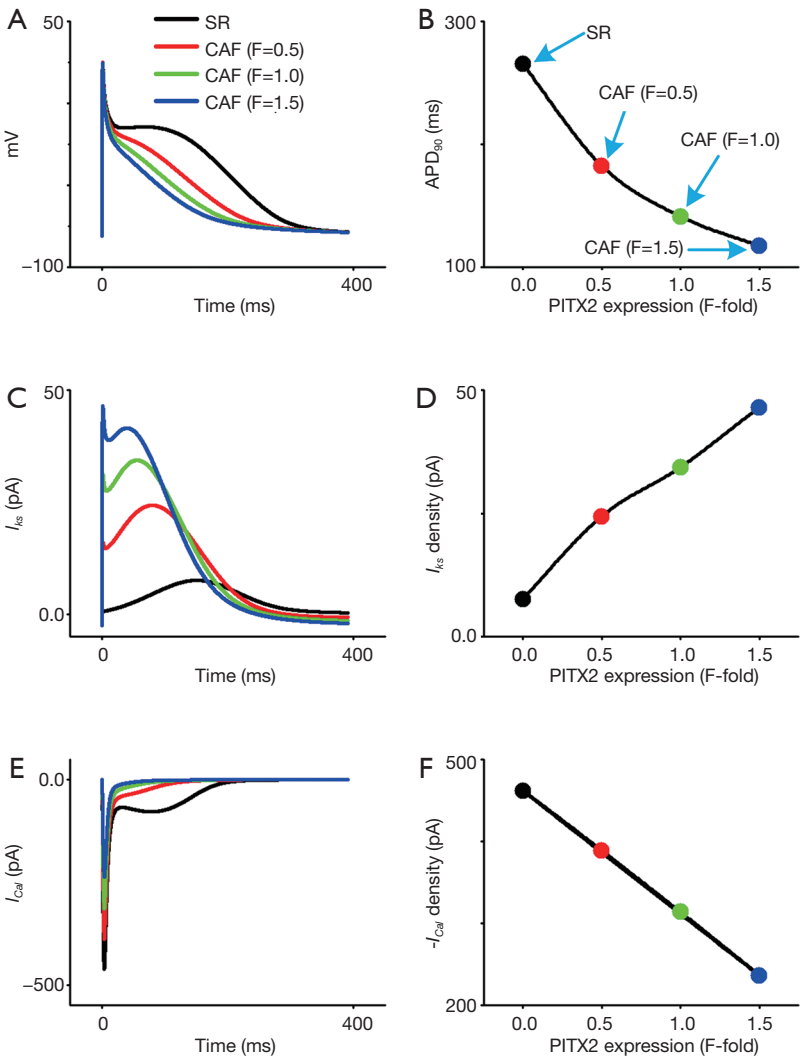

Figure 2 Simulated AP profiles and current traces under SR (black line), and CAF conditions where PITX2 expression is increased by 0.5-fold (F=0.5), 1.0-fold (F=1.0) and 1.5-fold (F=1.5). (A) AP profiles; (B) changes in APD as the modelling parameter F is increased from 0 (SR) to 1.5 (CAF) condition; (C) I_{Ks} profiles during APs; (D) I_{Ks} density increases with the increase of PITX2 expression; (E) I_{CaL} profiles during APs; (F) I_{CaL} density decreases with the increase of PITX2 expression. AP, action potential; SR, sinus rhythm; CAF, chronic atrial fibrillation; PITX2, paired-like homeodomain transcription factor 2; I_{Ks}, the slow delayed rectifier K^+ current; I_{CaL}, the L-type Ca^{2+} current; APD, AP duration.

of human atrial APs, 1D fiber tissues, 2D tissue sheets and 3D virtual human atria.

Results

Effects of the PITX2 overexpression on atrial APs

Increased I_{Ks} and reduced I_{CaL} due to the PITX2 overexpression abbreviated human atrial APs as shown in *Figure 2A*. The measured AP repolarization at 90% (APD_{90}) was 264.92 ms under SR condition. The increase in PITX2 expression caused a monotonic reduction in the APD_{90}. In details, the computed APD_{90} was 182.3, 141.26 and 117.11 ms, at CAF (F=0.5), CAF (F=1.0) and CAF (F=1.5), respectively (*Figure 2B*). The APD_{90} reduction was due to PITX2-induced changes in I_{Ks} and I_{CaL}. Under CAF conditions, the larger the PITX2 expression (indexed by F), the higher I_{Ks} density (*Figure 2C,D*) and the lower I_{CaL} density (*Figure 2E,F*). Since the PITX2 overexpression was seen to result in such an abbreviation of the APD_{90},

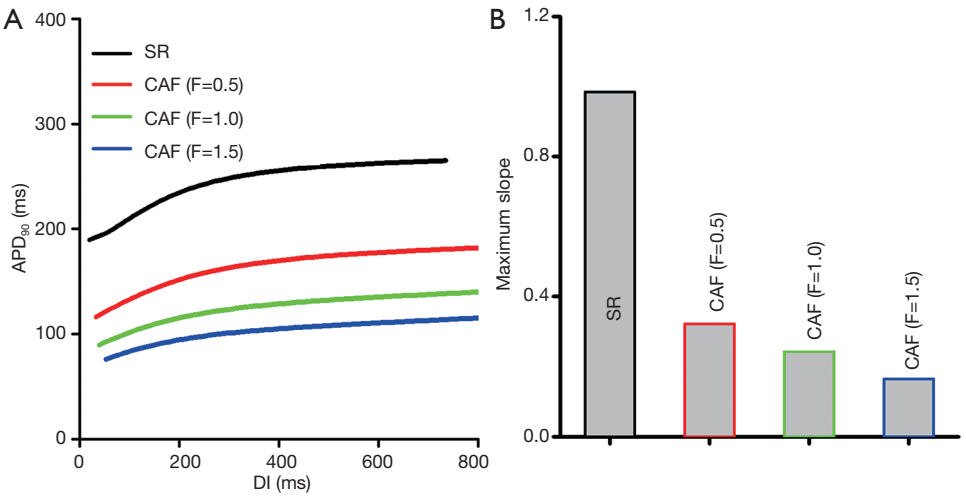

Figure 3 APDR curves under SR, CAF (F=0.5), CAF (F=1.0) and CAF (F=1.5) conditions. (A) APDR curves; (B) maximum slopes of the APDR curves. APDR, action potential duration restitution; SR, sinus rhythm; CAF, chronic atrial fibrillation; APD_{90}, AP repolarization at 90%; DI, diastolic interval.

effects of both I_{Ks} and I_{CaL} with altered proportions were investigated by a progressive increase in PITX2 expression (indexed by F).

Effects of the PITX2 overexpression on APD restitution (APDR) curves

Effects of changes in I_{Ks} and I_{CaL} due to the PITX2 overexpression on atrial APDR are shown in *Figure 3*. Across the range of diastolic intervals (DIs) studied, the computed APD_{90} under the CAF condition were smaller than that under the SR condition (*Figure 3A*). CAF conditions flattened APDR curves. The measured maximal APDR slopes were 0.98 (SR), 0.32 (F=0.5), 0.24 (F=1.0) and 0.16 (F=1.5) (*Figure 3B*). Such loss of rate-dependent adaptation of APD manifested by flattened APDR curves was similar to that observed in CAF patients (37), suggesting the increased ability of atrial cells to support high pacing rate electrical activity that can be pro-arrhythmic.

Effects of the PITX2 overexpression on CV and WL

PITX2 overexpression induced electrical remodeling led to a leftward shift of the measured CVR (*Figure 4A*). When the basic cycle length (BCL) is above 400 ms, there is no noticeable change in CV under the considered CAF conditions. When the BCL is below 400 ms, CV under the CAF condition is larger than in the SR condition. Therefore, the PITX2 overexpression facilitated conduction of excitation waves at higher rates that could not be conducted in SR tissue. The measured maximum excitation rate was 180 beats/min under the WT condition, which increased to 318, 498 and 558 beats/min in the F=0.5, F=1.0 and F=1.5 conditions, respectively.

Changes in I_{Ks} and I_{CaL} due to the PITX2 overexpression abbreviated WL as shown in *Figure 4B*. At the BCL =1,000 ms, the measured WL was 71.15 mm under the SR condition and 31.48 mm under the CAF (F=1.5) condition. So, the PITX2 overexpression favored to reentrant conduction of excitation in small tissues that could not be conducted under the SR condition. The measured size of 1D fiber tissue for reentry was 71.15 mm under the SR condition which decreased to 48.95, 37.96 and 31.48 mm in the F=0.5, F=1.0 and F=1.5 conditions, respectively.

Effects of the PITX2 overexpression on atrial tissue temporal and spatial vulnerability

The measured spatial vulnerability of atrial tissue in the 2D model is shown in *Figure 5*. Under the SR condition, the computed minimal substrate length required to induce and sustain reentry was 62 mm (*Figure 5A*). Under the CAF conditions, the substrate length decreased to 35 mm (by 43.5%) when F=0.5, to 28 mm (by 54.8%) when F=1.0, and to 22 mm in the F=1.5 case (*Figure 5B*). Thus, the PITX2 overexpression caused a marked reduction in the substrate

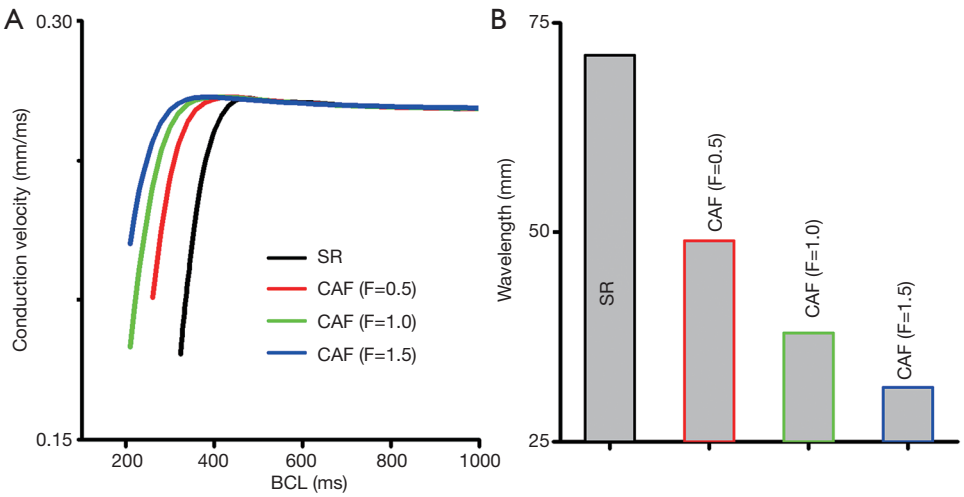

Figure 4 CVR and WL. (A) CVR curves under SR, CAF (F=0.5), CAF (F=1.0) and CAF (F=1.5) conditions; (B) spatial WL under SR, CAF (F=0.5), CAF (F=1.0) and CAF (F=1.5) conditions. CVR, conduction velocity restitution; WL, wavelength; SR, sinus rhythm; CAF, chronic atrial fibrillation; BCL, basic cycle length.

size, demonstrating a marked increase in tissue susceptibility to arrhythmogenesis.

The temporal vulnerability of atrial tissue was quantified by the VW (*Figure 5C*). Compared with the SR condition, effects of the PITX2 overexpression on VW were almost negligible.

Effects of the PITX2 overexpression on dynamic behavior of re-entrant excitation waves in 2D model

Alterations in I_{Ks} and I_{CaL} due to the PITX2 overexpression stabilized re-entrant spiral waves, leading to sustained re-entrant excitation in a limited atrial model. Under the SR condition, the initiated spiral wave was unstable. Its tip meandered in a large area, which led to self-termination when it meandered out of the tissue boundaries or collided with its own repolarization tail. The measured lifespan (LS) of spiral waves was 1.1 s in the SR condition. Power spectrum analysis of the recorded local electrical activity revealed a peak frequency of 3.0 Hz for SR. Under intermediate CAF conditions (F=0.5 and F=1.0), re-entrant waves were stable, persistent and had limited meander throughout the 10 s simulation. The dominant frequency reached to 5.3 and 8.3 Hz for F=0.5 and F=1.0, respectively. Similar behaviors of spiral waves were observed under the CAF (F=1.5) condition (*Figure 6*).

Scroll waves in 3D atria

To examine whether PITX2-induced changes in I_{Ks} and I_{CaL} facilitate sustained re-entry in 3D anatomical atrial geometry, further simulations were conducted using a 3D human atrial model. As shown in *Figure 7*, spiral waves initiated by cross-field stimulation protocol self-terminated within 1.0 s under the SR condition. However, spiral waves interacted with the complex geometry of atrial tissue and broke into multiple wavelets in the case of CAF (F=1.5). These scroll waves sustained within 5.0 s and the dominant frequency reached to 7.6 Hz.

A quantitative summary of the effects of the PITX2 overexpression on human atrial electrical activity is listed in *Table 1*.

Discussion

To our knowledge, this is the first in silico study investigating the pro-arrhythmic effects of electrical remodeling due to PITX2 overexpression based on experimental data from SR and CAF patients. Our major findings are the following: (I) PITX2-induced changes in I_{Ks} and I_{CaL} led to APD shortening and APDR curves flattening, (II) These consequent changes in cellular electrophysiology

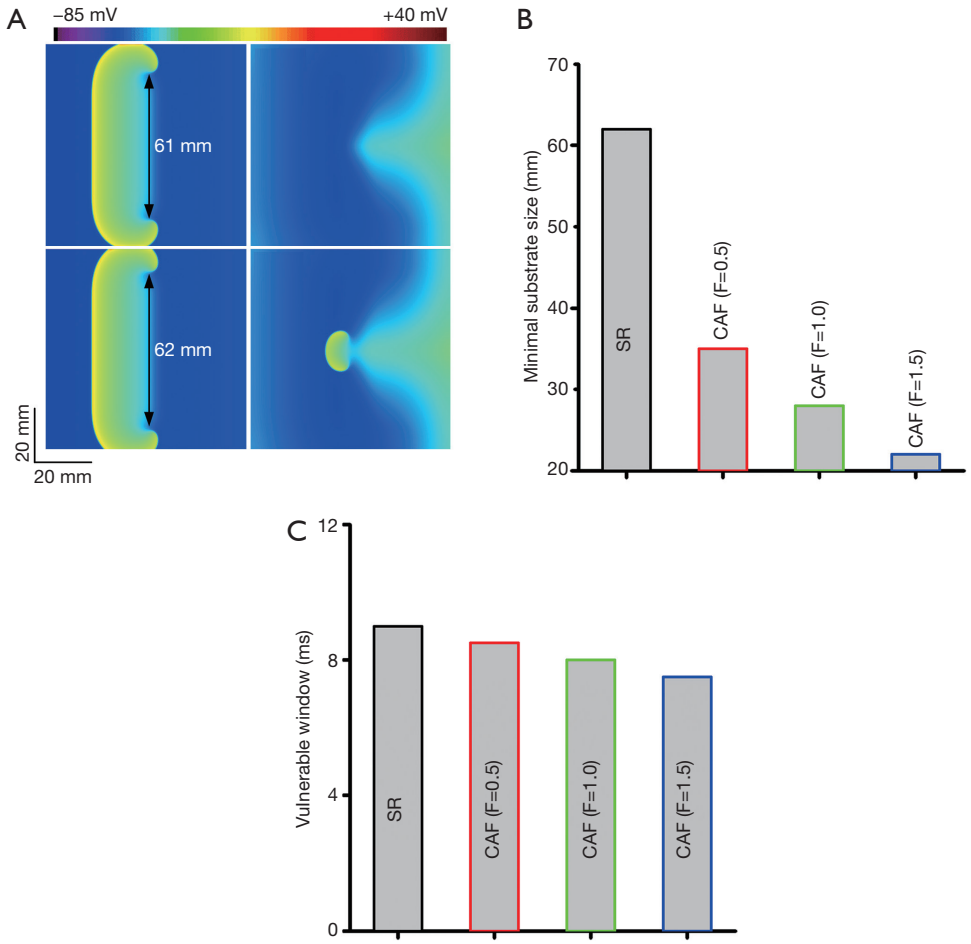

Figure 5 Critical length of the minimal substrate size for re-entry in 2D sheets. (A) illustration of the minimal substrate size required to induce a pair of re-entrant circuits in homogeneous 2D sheets; (B) critical length under SR, CAF (F=0.5), CAF (F=1.0) and CAF (F=1.5) conditions. The critical length under CAF conditions was dramatically shorter than that under the SR condition; (C) VW under SR and CAF conditions. 2D, two-dimensional; SR, sinus rhythm; CAF, chronic atrial fibrillation; VW, vulnerable window.

decreased WL and modulated CV, facilitating atrial conduction at high rates in atrial tissue model, and (III) alterations in I_{Ks} and I_{CaL} arising from PITX2 overexpression increased tissue spatial vulnerability to re-entry and stabilized spiral waves. Therefore, PITX2-induced changes in I_{Ks} and I_{CaL} provide substrates required for initiation and maintenance of AF.

PITX2 alterations and AF

Genome-wide association studies have provided evidence of a genetic contribution to AF. AF variants adjacent to PITX2 were first identified by Gudbjartsson *et al.* (19). The association between PITX2 and AF was further confirmed in many populations (38) and also was reported for its role in left-right asymmetry of cardiac development, including alterations in the development of sinoatrial node (39) and myocardial sleeves of the pulmonary veins (26). However, a recent study in adult mouse models suggested PITX2 plays a critical function in maintaining atrial rhythm (24). Chinchilla *et al.* first demonstrated the association between loss of function of PITX2 and AF in human patients (40), whereas gain of function of PITX2 was observed in human right (16) and left (41) atrial appendages obtained from AF patients. These differences may be attributed to patient characteristics and type of AF. In the study of Syeda *et al.* (42) and Gore-Panter *et al.* (43), PITX2 mRNA varied from low to high levels in human left atrial appendages harvested

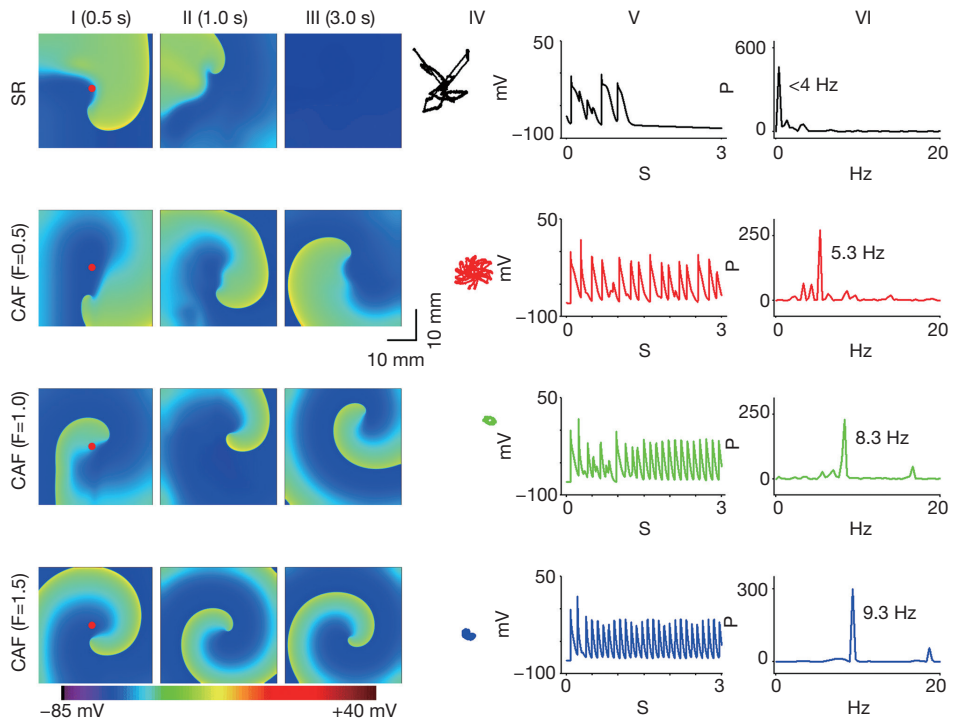

Figure 6 Simulation of spiral waves in 2D model of human right atrium. Top panels show results from 2D re-entrant wave simulation under SR condition; the second, third and fourth rows of panels show results from CAF (F=0.5), CAF (F=1.0) and CAF (F=1.5) conditions, respectively. Frames from the 2D simulation at time t=0.5 s (column I), t=1.0 s (column II) and t=3.0 s (column III) are shown. Column IV shows the re-entrant wave tip trajectories. Column V shows AP traces of localized electrical excitations. Column VI shows dominant frequencies. 2D, two-dimensional; SR, sinus rhythm; CAF, chronic atrial fibrillation; AP, action potential.

from AF patients which were subdivided into several groups based on type of AF or history of AF. Therefore, Pérez-Hernández *et al.* measured PITX2 mRNA expression in isolated myocytes from right atrial appendages obtained from patients in SR and patients diagnosed with CAF (>6 months at the time of surgery) (16). Their experiments showed that PITX2 mRNA expression in CAF myocytes was ~1.5-fold greater than in SR cells (16). Based on experimental data of Pérez-Hernández *et al.*, we predicted the pro-arrhythmic effects of the PITX2 overexpression in this study.

Mechanisms of pro-fibrillation of the PITX2 overexpression

Down-regulation of I_{CaL} and up-regulation of I_{Ks} are hallmarks of electrical remodeling in AF patients and mainly cause APD shortening (44). In the case of the PITX2 overexpression, I_{Ks} increased and I_{CaL} decreased with the increase in PITX2 expression. In turn, changes in I_{Ks} and I_{CaL} abbreviated APD and effective refractory period (ERP) at the single cell level. This shortened ERP can cause WL abbreviation and allow spiral waves to persist within a limited tissue. In CAF patients (45), electrical remodeling induced by long-lasting AF (46) abbreviated APD, and shifted downward and flattened APDR (47), facilitating the long-term stabilization of CAF (48). This is consistent with our simulations that sustained spiral waves were observed in CAF conditions.

The development of CAF in patients with overexpressed PITX2 may be attributed to the increased vulnerability of atrial tissue to spiral waves. On the one hand, tissue vulnerability to re-entry can be indexed by WL. WL, which is defined as the product of CV and ERP, determined the substrate size to enable re-entry to be persisted. In this study, changes in I_{Ks} and I_{CaL} due to the PITX2 overexpression have been shown to shorten APD and ERP at the single cell level, and to abbreviate WL at the tissue level. Consequently, the critical size of the re-entrant

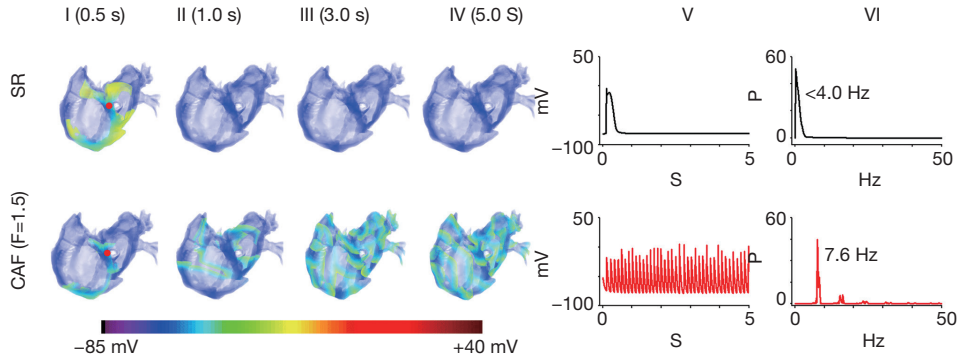

Figure 7 Simulation of spiral waves in 3D virtual human atrium. Top panels show results from 3D re-entrant wave simulation under SR condition and bottom panels show results under CAF (F=1.5). Column I, II, III and IV show frames at t=0.5, 1.0, 3.0 and 5.0 s, respectively. Column V shows AP traces of localized electrical excitations. Column VI shows dominant frequencies. 3D, three-dimensional; SR, sinus rhythm; CAF, chronic atrial fibrillation; AP, action potential.

Table 1 Quantitative summary of the effects of PITX2 overexpression on human atrial electrical activity

Model	Quantity	SR (F=0.0)	CAF (F=0.5)	CAF (F=1.0)	CAF (F=1.5)
Cell	Resting potential (mV)	–80.8	–80.8	–80.8	–80.8
	APD_{30} (ms)	9.9	8.4	6.9	6.0
	APD_{50} (ms)	158.7	74.0	42.9	27.7
	APD_{90} (ms)	264.9	182.3	141.3	117.1
	Overshoot (ms)	24.9	24.8	24.6	24.5
	dV/dt_{max} (mV/ms)	210.07	209.97	209.86	209.76
	APDR maximal slope	0.98	0.32	0.24	0.16
1D	CV (mm/ms)	0.27	0.27	0.27	0.27
	WL (mm)	71.15	48.95	37.96	31.48
	VW (ms)	9.0	8.5	8.1	7.5
2D	LS (s)	1.1	>10	>10	>10
	Minimal substrate size (mm)	62	35	28	22
	Domain frequency (Hz)	3.5	5.3	8.3	9.3
	Tip meander area (mm^2)	460	131	5.7	5.3
3D	LS (s)	<1	–	–	>5
	Domain frequency (Hz)	<4.0	–	–	7.6

PITX2, paired-like homeodomain transcription factor 2; SR, sinus rhythm; CAF, chronic atrial fibrillation; APD_{90}, AP repolarization at 90%; APDR, action potential duration restitution; CV, conduction velocity; WL, wavelength; VW, vulnerable window; LS, lifespan.

substrate markedly decreased and atrial tissue susceptibility to maintain spiral waves was increased. This observation is consistent with findings from the study by Padeletti *et al.*, that the WL index was shorter in AF patients than in SR group (49). On the other hand, tissue susceptibility to re-entry can also be indexed by VW. Within VW, a test stimulus applied to the refractory tail of a conditioning excitation wave can evoke unidirectional conduction block necessary to re-entry genesis (50). In this study, changes in I_{Ks} and I_{CaL} due to PITX2 overexpression had no effects

on VW. Therefore, in the case of PITX2 overexpression, the increased susceptibility of AF can be attributed to APD shortening and WL abbreviation.

A pro-arrhythmic effect of abbreviated atrial APD with CAF has also observed in simulations (8,9,36,48,51-54). Computer modelling has shown that CAF-induced electrical remodeling reduced APD (9,54) and flattened APDR curves (8,36,52,53). In addition, CAF-induced electrical remodeling also decreased WL and facilitated persistent spiral waves (8,36,51-53). These observations for CAF-induced electrical remodeling, which includes upregulated potassium currents and downregulated calcium currents (8,9,36,48,51-54), are qualitatively similar to those observed here for the PITX2 overexpression. Therefore, the findings of the present study add to the growing weight to evidence implicating APD shortening in facilitating AF maintenance.

Limitations

The limitations of the original model developed by Courtemanche *et al.* have been addressed elsewhere (35). Here, several limitations special to the present study are summarized. Firstly, expect for alterations in I_{Ks} and I_{CaL} we did not considered remodeling in other ion channels, calcium handling and cell-to-cell coupling, which influences the initiation and maintenance of AF (8,9,31,52,55,56). Secondly, there are three pedigrees of human atrial cell models: Courtemanche-Colman (8,35), Nygren-Maleckar-Koivumäki-Skibsbye (52,57) and Grandi-Voigt-Schmidt (9,58) lineages. Although APD shortening was observed under CAF conditions using human atrial cell models developed by Courtemanche *et al.*, Skibsbye *et al.*, and Grandi *et al.* (*Figure S1*), the computed APD is different between these models (*Table S1*) which are based on varying dataset and assumptions (51,59). Finally, the multicellular tissue model was assumed to be homogeneous in cellular electrical properties and cell-to-cell coupling. However, the intrinsic heterogeneity in cellular electrical properties and intercellular coupling influences the genesis of spiral waves (60-66). For the present study, omitting the intrinsic heterogeneity is useful to understand the mechanisms underlying AF arising from the PITX2 overexpression, in that changes in the spatial-temporal patterns of spiral waves can be attributed with confidence to the implemented modifications to I_{Ks} and I_{CaL} due to the PITX2 upregulation. Although these potential limitations are important in the present study, they may not influence our conclusions drawn from simulated results on the mechanisms by which the I_{Ks} increase and I_{CaL} decrease due to the PITX2 overexpression can increase the risk of CAF.

PITX2 and AF-relevance to previous studies

Gain-of-function/loss-of-function of PITX2 has been found to be associated with colorectal cancer (67), Axenfeld-Rieger syndrome (68-70) and AF (16,40-43,71,72) in human. The variability of PITX2 in patients suggesting that there is a critical level of PITX2 for normal functions in human. There are >50 mutations related with the Axenfeld-Rieger syndrome in which most are loss-of-function mutations and 6 of them are gain-of-function mutations (68-70). Besides, both under- and overexpression of PITX2 also was also associated with high susceptibility to AF. A number of previous studies have shown expression levels of PITX2 are reduced in the left atrium in humans (40,42,43) and transgenic mice (24,29,40), or with loss-of-function mutations (71,73). However, PITX2 expression has been found to be increased in the left atrium (41) and in right atrial myocytes (16), from AF patients, or with the gain-of-function mutation p.Met207Val (10,72). In agreement with CAF patients with overexpressed PITX2 (16), we have predicted increased I_{Ks} and reduced I_{CaL} arising from the PITX2 overexpression shortened atrial APD and increased atrial susceptibility to arrhythmia.

Previous modelling studies have demonstrated that distinct conditions (including PITX2 up-regulation and down-regulation) can have variable effects on ion channels, AP morphologies and electrical waves, depending on variations in experimental data. For PITX2 down-regulation conditions, Syeda *et al.* modelled PITX2 deficiency by considering two electrical targets and investigated its effect on AP properties (42). Simulated results demonstrated that PITX2 deficiency resulted in enhanced post-repolarization refractoriness. In addition to all electrical targets (i.e., I_{Na}, I_{Ks}, I_{K1} and I_{CaL}), we considered changes to the subcellular calcium handling properties (i.e., *RyR* and *SERCA*) in our single-cell models and simulated data indicated that PITX2 deficiency might modulate resting membrane potential and promote triggered activities (31). Furthermore, we introduced structural remodeling (including cell-to-cell coupling and fibroblasts) into our multiscale models and assessed the role of each remodeled target in AF. Our findings support this notion that PITX2 deficiency may promote reentry and/or ectopic activity (74). Recently, the PITX2 up-regulation in AF patients was

also observed. And the potential impact of the gain-of-function PITX2 mutation p.Met207Val on atrial electrical activity was investigated by integrating changes to ionic channel currents (I_{NaL}, I_{Ks}, and I_{Kr}) and intercellular electrical coupling. Our data indicated that APD shortening and slow conduction may increase atrial susceptibility to familial AF arising from the PITX2 p.Met207Val mutation (10). By contrast, in the present study, APD shortening due to PITX2-induced alterations in ion channels (I_{Ks} and I_{CaL}) and unaltered conduction at the baseline also contribute to AF but with a different mechanism.

Accumulating evidence places particular emphasis on AF-induced electrical remodeling or electrophysiological modification due to PITX2 defects, in producing a pro-fibrillatory reduction in APD (29). The present study is both consistent with and extends this notion, indicating a marked functional impact of gain-of-function of PITX2 on atrial cell and tissue electrophysiology that would promote susceptibility to AF. The general incidence of AF increases with age (75). The previous study of Scridon *et al.* have shown that PITX2 expressions showed a progressive, age-dependent change and were negatively correlated with both age and heart weight in hypertensive rats (76). It indicated a possible temporal relationship between the PITX2 alteration and arrhythmia onset, suggesting PITX2 alteration is an age-dependent process that starts before the occurrence of arrhythmias. And Lozano-Velasco *et al.* identified a complex regulatory network orchestrated by PITX2, demonstrating a dose-dependent relation between PITX2 expression and the expression of AF susceptibility genes (77). Importantly, human right atrial myocytes from CAF patients have shown PITX2 expression increases and this increase correlates with the I_{Ks} increase and I_{CaL} decrease that characterize CAF-induced electrical remodeling (16,78), demonstrating the substrate for arrhythmogenesis in these CAF patients is dependent upon electrical remodeling modulated by the PITX2 expression in a dose-dependent manner. Our data are consistent with this. They indicate that in the case of PITX2 overexpression, the reduction in APD and the increase in spatial vulnerability to arrhythmia contribute to the substrate for maintaining AF through stabilizing re-entry. Therefore, our study substantiates a causative link between the PITX2 overexpression and arrhythmogenesis.

Acknowledgments

We would thank Miss Shaleka Agrawal for giving our valuable suggestions.

Funding: This work was supported by the National Natural Science Foundation of China (No. 61901192), the National Key R&D Program of China (No. 2019YFC0120100 and 2019YFC0121900) and the Science and Technology Planning Project of Guangdong Province (No. 2015B020214004 and No. 2015B020233010).

Footnote

Conflicts of Interest: The authors have no conflicts of interest to declare.

Ethical Statement: The authors are accountable for all aspects of the work in ensuring that questions related to the accuracy or integrity of any part of the work are appropriately investigated and resolved. This simulation study is not involved in any ethical information.

References

1. Weng LC, Preis SR, Hulme OL, et al. Genetic predisposition, clinical risk factor burden, and lifetime risk of atrial fibrillation. Circulation 2018;137:1027-38.
2. Heijman J, Guichard JB, Dobrev D, et al. Translational challenges in atrial fibrillation. Circ Res 2018;122:752-73.
3. Nattel S. Paroxysmal atrial fibrillation and pulmonary veins: relationships between clinical forms and automatic versus re-entrant mechanisms. Can J Cardiol 2013;29:1147-9.
4. Bai J, Wang K, Li Q, et al. Pro-arrhythmogenic effects of CACNA1C G1911R mutation in human ventricular tachycardia: insights from cardiac multi-scale models. Sci Rep 2016;6:31262.
5. Haïssaguerre M, Jaïs P, Shah DC, et al. Spontaneous initiation of atrial fibrillation by ectopic beats originating in the pulmonary veins. N Engl J Med 1998;339:659-66.
6. Bai J, Wang K, Liu Y, et al. Computational cardiac modeling reveals mechanisms of ventricular

arrhythmogenesis in long QT syndrome type 8: CACNA1C R858H mutation linked to ventricular fibrillation. Front Physiol 2017;8:771.
7. Bai J, Yin R, Wang K, et al. Mechanisms underlying the emergence of post-acidosis arrhythmia at the tissue level: a theoretical study. Front Physiol 2017;8:195.
8. Colman MA, Aslanidi OV, Kharche S, et al. Pro arrhythmogenic effects of atrial fibrillation-induced electrical remodelling: insights from the three-dimensional virtual human atria. J Physiol 2013;591:4249-72.
9. Grandi E, Pandit SV, Voigt N, et al. Human atrial action potential and Ca2+ model: sinus rhythm and chronic atrial fibrillation. Circ Res 2011;109:1055-66.
10. Bai J, Lu Y, Zhang H. In silico study of the effects of anti-arrhythmic drug treatment on sinoatrial node function for patients with atrial fibrillation. Sci Rep 2020;10:305.
11. Thijssen VL, Ausma J, Borgers M. Structural remodelling during chronic atrial fibrillation: act of programmed cell survival. Cardiovasc Res 2001;52:14-24.
12. Roselli C, Chaffin MD, Weng LC, et al. Multi-ethnic genome-wide association study for atrial fibrillation. Nat Genet 2018;50:1225-33.
13. Benjamin EJ, Rice KM, Arking DE, et al. Variants in ZFHX3 are associated with a trial fibrillation in individuals of European ancestry. Nat Genet 2009;41:879-81.
14. Ellinor PT, Lunetta KL, Albert CM, et al. Meta-analysis identifies six new susceptibility loci for atrial fibrillation. Nat Genet 2012;44:670-5.
15. Sinner MF, Tucker NR, Lunetta KL, et al. Integrating genetic, transcriptional, and functional analyses to identify 5 novel genes for atrial fibrillation. Circulation 2014;130:1225-35.
16. Pérez-Hernández M, Matamoros M, Barana A, et al. Pitx2c increases in atrial myocytes from chronic atrial fibrillation patients enhancing IKs and decreasing ICa,L. Cardiovasc Res 2016;109:431-41.
17. Darbar D, Roden D. Genetic mechanisms of atrial fibrillation: impact on response to treatment. Nat Rev Cardiol 2013;10:317-29.
18. Sutanto H, Dobrev D, Heijman J. Genome-wide association studies of atrial fibrillation: Finding meaning in the life of risk loci. Int J Cardiol Heart Vasc 2019;24:100397.
19. Gudbjartsson DF, Arnar DO, Helgadottir A, et al. Variants conferring risk of atrial fibrillation on chromosome 4q25. Nature 2007;448:353-7.
20. Viviani Anselmi C, Novelli V, Roncarati R, et al. Association of rs2200733 at 4q25 with atrial flutter/fibrillation diseases in an Italian population. Heart 2008;94:1394-6.
21. Shi L, Li C, Wang C, et al. Assessment of association of rs2200733 on chromosome 4q25 with atrial fibrillation and ischemic stroke in a Chinese Han population. Hum Genet 2009;126:843-9.
22. Kääb S, Darbar D, Van Noord C, et al. Large scale replication and meta-analysis of variants on chromosome 4q25 associated with atrial fibrillation. Eur Heart J 2009;30:813-9.
23. Parvez B, Shoemaker MB, Muhammad R, et al. Common genetic polymorphism at 4q25 locus predicts atrial fibrillation recurrence after successful cardioversion. Heart Rhythm 2013;10:849-55.
24. Nadadur RD, Broman MT, Boukens B, et al. Pitx2 modulates a Tbx5-dependent gene regulatory network to maintain atrial rhythm. Sci Transl Med 2016;8:354ra115.
25. Boldt LH, Posch MG, Perrot A, et al. Mutational analysis of the PITX2 and NKX2-5 genes in patients with idiopathic atrial fibrillation. Int J Cardiol 2010;145:316-7.
26. Mommersteeg MT, Brown NA, Prall OW, et al. Pitx2c and Nkx2-5 are required for the formation and identity of the pulmonary myocardium. Circ Res 2007;101:902-9.
27. Ritchie MD, Rowan S, Kucera G, et al. Chromosome 4q25 variants are genetic modifiers of rare ion channel mutations associated with familial atrial fibrillation. J Am Coll Cardiol 2012;60:1173-81.
28. Syeda F, Kirchhof P, Fabritz L. PITX2-dependent gene regulation in atrial fibrillation and rhythm control. J Physiol 2017;595:4019-26.
29. Kirchhof P, Kahr PC, Kaese S, et al. PITX2c is expressed in the adult left atrium, and reducing Pitx2c expression promotes atrial fibrillation inducibility and complex changes in gene expression. Circ Cardiovasc Genet 2011;4:123-33.
30. Tao Y, Zhang M, Li L, et al. Pitx2, an atrial fibrillation predisposition gene, directly regulates ion transport and intercalated disc genes. Circ Cardiovasc Genet 2014;7:23-32.
31. Bai J, Gladding PA, Stiles MK, et al. Ionic and cellular mechanisms underlying TBX5/PITX2 insufficiency-induced atrial fibrillation: Insights from mathematical models of human atrial cells. Sci Rep 2018;8:15642.
32. Bai J, Wang K, Zhang H. Potential pathogenesis discovery of arrhythmia based on cardiac electrophysiological models: research progress. Prog Biochem Biophys 2016;43:128-40.
33. Bai J, Xie S, Wang K, et al. Simulation Research on Early

Afterdepolarizations-mediated Ventricular Fibrillation Based on a Heart Model. Prog Biochem Biophys 2015;42:955-61.
34. Liu H, Bai J, Wang K, et al. Simulation study of ventricular arrhythmia in post acidosis. Prog Biochem Biophys 2016;43:716-24.
35. Courtemanche M, Ramirez RJ, Nattel S. Ionic mechanisms underlying human atrial action potential properties: insights from a mathematical model. Am J Physiol 1998;275:H301-21.
36. Pandit SV, Berenfeld O, Anumonwo JM, et al. Ionic determinants of functional reentry in a 2-D model of human atrial cells during simulated chronic atrial fibrillation. Biophys J 2005;88:3806-21.
37. Narayan SM, Franz MR, Clopton P, et al. Repolarization alternans reveals vulnerability to human atrial fibrillation. Circulation 2011;123:2922-30.
38. Lubitz SA, Sinner MF, Lunetta KL, et al. Independent susceptibility markers for atrial fibrillation on chromosome 4q25. Circulation 2010;122:976-84.
39. Wang J, Bai Y, Li N, et al. Pitx2-microRNA pathway that delimits sinoatrial node development and inhibits predisposition to atrial fibrillation. Proc Natl Acad Sci U S A 2014;111:9181-6.
40. Chinchilla A, Daimi H, Lozano-Velasco E, et al. PITX2 insufficiency leads to atrial electrical and structural remodeling linked to arrhythmogenesis. Circ Cardiovasc Genet 2011;4:269-79.
41. Gore-Panter SR, Hsu J, Hanna P, et al. Atrial fibrillation associated chromosome 4q25 variants are not associated with PITX2c expression in human adult left atrial appendages. PLoS One 2014;9:e86245.
42. Syeda F, Holmes AP, Ting YY, et al. PITX2 modulates atrial membrane potential and the antiarrhythmic effects of sodium-channel blockers. J Am Coll Cardiol 2016;68:1881-94.
43. Gore-Panter SR, Hsu J, Barnard J, et al. PANCR, the PITX2 adjacent noncoding RNA, is expressed in human left atria and regulates PITX2c expression. Circ Arrhythm Electrophysiol 2016;9:e003197.
44. Van Wagoner DR, Pond AL, Lamorgese M, et al. Atrial L-type Ca2+ currents and human atrial fibrillation. Circ Res 1999;85:428-36.
45. Lee G, Kumar S, Teh A, et al. Epicardial wave mapping in human long-lasting persistent atrial fibrillation: transient rotational circuits, complex wavefronts, and disorganized activity. Eur Heart J 2014;35:86-97.
46. Lau CP, Tse HF. Electrical remodelling of chronic atrial fibrillation. Clin Exp Pharmacol Physiol 1997;24:982-3.
47. Franz MR, Karasik PL, Li C, et al. Electrical remodeling of the human atrium: similar effects in patients with chronic atrial fibrillation and atrial flutter. J Am Coll Cardiol 1997;30:1785-92.
48. González de la Fuente M, Barana A, Gómez R, et al. Chronic atrial fibrillation up-regulates 1-Adrenoceptors affecting repolarizing currents and action potential duration. Cardiovasc Res 2013;97:379-88.
49. Padeletti L, Michelucci A, Giovannini T, et al. Wavelength index at three atrial sites in patients with paroxysmal atrial fibrillation. Pacing Clin Electrophysiol 1995;18:1266-71.
50. Shaw RM, Rudy Y. The vulnerable window for unidirectional block in cardiac tissue: characterization and dependence on membrane excitability and intercellular coupling. J Cardiovasc Electrophysiol 1995;6:115-31.
51. Wilhelms M, Hettmann H, Maleckar MMC, et al. Benchmarking electrophysiological models of human atrial myocytes. Front Physiol 2013;3:487.
52. Koivumäki JT, Seemann G, Maleckar MM, et al. In silico screening of the key cellular remodeling targets in chronic atrial fibrillation. PLoS Comput Biol 2014;10:e1003620.
53. Lee YS, Hwang M, Song JS, et al. The contribution of ionic currents to rate-dependent action potential duration and pattern of reentry in a mathematical model of human atrial fibrillation. PLoS One 2016;11:e0150779.
54. Adeniran I, Maciver DH, Garratt CJ, et al. Effects of persistent atrial fibrillation-induced electrical remodeling on atrial electro-mechanics–insights from a 3D model of the human atria. PLoS One 2015;10:e0142397.
55. Seemann G, Höper C, Sachse FB, et al. Heterogeneous three-dimensional anatomical and electrophysiological model of human atria. Philos Trans A Math Phys Eng Sci 2006;364:1465-81.
56. Krogh-Madsen T, Abbott G W, Christini DJ. Effects of electrical and structural remodeling on atrial fibrillation maintenance: a simulation study. PLoS Comput Biol 2012;8:e1002390.
57. Skibsbye L, Jespersen T, Christ T, et al. Refractoriness in human atria: time and voltage dependence of sodium channel availability. J Mol Cell Cardiol 2016;101:26-34.
58. Voigt N, Heijman J, Trausch A, et al. Impaired Na+-dependent regulation of acetylcholine-activated inward-rectifier K+ current modulates action potential rate dependence in patients with chronic atrial fibrillation. J Mol Cell Cardiol 2013;61:142-52.
59. Vagos M, van Herck IGM, Sundnes J, et al. Computational modeling of electrophysiology and pharmacotherapy of

atrial fibrillation: recent advances and future challenges. Front Physiol 2018;9:1221.
60. Hansen BJ, Zhao J, Li N, et al. Human atrial fibrillation drivers resolved with integrated functional and structural imaging to benefit clinical mapping. JACC Clin Electrophysiol 2018;4:1501-15.
61. Stephenson RS, Atkinson A, Kottas P, et al. High resolution 3-Dimensional imaging of the human cardiac conduction system from microanatomy to mathematical modeling. Sci Rep 2017;7:7188.
62. Zhao J, Hansen BJ, Wang Y, et al. Three-dimensional integrated functional, structural, and computational mapping to define the structural "fingerprints" of heart-specific atrial fibrillation drivers in human heart ex vivo. J Am Heart Assoc 2017;6:e005922.
63. Hansen BJ, Zhao J, Fedorov VV. Fibrosis and atrial fibrillation: computerized and optical mapping: a view into the human atria at submillimeter resolution. JACC Clin Electrophysiol 2017;3:531-46.
64. Li N, Csepe TA, Hansen BJ, et al. Adenosine-induced atrial fibrillation: localized reentrant drivers in lateral right atria due to heterogeneous expression of adenosine A1 receptors and GIRK4 subunits in the human heart. Circulation 2016;134:486-98.
65. Zhao J, Hansen BJ, Csepe TA, et al. Integration of high-resolution optical mapping and 3-dimensional micro-computed tomographic imaging to resolve the structural basis of atrial conduction in the human heart. Circ Arrhythm Electrophysiol 2015;8:1514-7.
66. Hansen BJ, Zhao J, Csepe TA, et al. Atrial fibrillation driven by micro-anatomic intramural re-entry revealed by simultaneous sub-epicardial and sub-endocardial optical mapping in explanted human hearts. Eur Heart J 2015;36:2390-401.
67. Hirose H, Ishii H, Mimori K, et al. The significance of PITX2 overexpression in human colorectal cancer. Ann Surg Oncol 2011;18:3005-12.
68. Tümer Z, Bach-Holm D. Axenfeld-Rieger syndrome and spectrum of PITX2 and FOXC1 mutations. Eur J Hum Genet 2009;17:1527-39.
69. Priston M, Kozlowski K, Gill D, et al. Functional analyses of two newly identified PITX2 mutants reveal a novel molecular mechanism for Axenfeld-Rieger syndrome. Hum Mol Genet 2001;10:1631-8.
70. Saadi I, Toro R, Kuburas A, et al. An unusual class of PITX2 mutations in Axenfeld-Rieger syndrome. Birth Defects Res A Clin Mol Teratol 2006;76:175-81.
71. Qiu XB, Xu YJ, Li RG, et al. PITX2C loss-of-function mutations responsible for idiopathic atrial fibrillation. Clinics 2014;69:15-22.
72. Bai J, Lu Y, Lo A, et al. Proarrhythmia in the p.Met207Val PITX2c-linked familial atrial fibrillation-insights from modeling. Front Physiol 2019;10:1314.
73. Wang J, Xin YF, Xu WJ, et al. Prevalence and spectrum of PITX2c mutations associated with congenital heart disease. DNA Cell Biol 2013;32:708-16.
74. Bai J, Lo A, Gladding PA, et al. In silico investigation mechanisms underlying atrial fibrillation due to impaired Pitx2. PLoS Comput Biol 2020;16:e1007678.
75. Nattel S. New ideas about atrial fibrillation 50 years on. Nature 2002;415:219-26.
76. Scridon A, Fouilloux-Meugnier E, Loizon E, et al. Long-standing arterial hypertension is associated with Pitx2 down-regulation in a rat model of spontaneous atrial tachyarrhythmias. Europace 2015;17:160-5.
77. Lozano-Velasco E, Hernández-Torres F, Daimi H, et al. Pitx2 impairs calcium handling in a dose-dependent manner by modulating Wnt signalling. Cardiovasc Res 2016;109:55-66.
78. Kharche S, Adeniran I, Stott J, et al. Pro-arrhythmogenic effects of the S140G KCNQ1 mutation in human atrial fibrillation-insights from modelling. J Physiol 2012;590:4501-14.

Cite this article as: Bai J, Lu Y, Lo A, Zhao J, Zhang H. PITX2 upregulation increases the risk of chronic atrial fibrillation in a dose-dependent manner by modulating I_{Ks} and I_{CaL}—insights from human atrial modelling. Ann Transl Med 2020;8(5):191. doi: 10.21037/atm.2020.01.90

AP simulation at the single cell level

Three models of human atrial electrophysiology were used to represent the current pedigrees of human atrial cell models in the present study. The membrane potential was computed according to the following differential equation:

$$\frac{dV}{dt} = -\frac{I_{ion} + I_{stim}}{C_m} \quad [9]$$

Where t is time, I_{ion} is the total sum of ionic currents, I_{stim} is a stimulus current and C_m is the membrane capacitance.

APD_{90} was defined as AP repolarization at 90%. APDR was measured using the S1-S2 protocol, which includes 30 S1 stimuli and 1 S2 stimulus. These restitution curves were generated by plotting the APD_{90} against the corresponding DI.

1D simulations

The modified CRN cell model was integrated into a homogeneous 1D model to simulate AP propagation. The 1D fiber tissue consists of 200 nodes and the membrane potential was computed according to the following equation:

$$\frac{dV}{dt} = -\frac{I_{ion} + I_{stim}}{C_m} + D \cdot \left(\frac{\delta^2 V}{\delta x^2} \right) \quad [10]$$

where t (ΔT=0.005 ms) is time, the space step (Δx) is set to be 0.1 mm, D (0.031 mm^2/ms) is a diffusion coefficient that leads to a CV of 0.27 mm/ms for a planar wave under the SR condition, and I_{stim}(amplitude: –80 nA/pF and duration: 1 ms) is a stimulus current. The external stimulus was applied to the three nodes at the end of the fiber tissue.

CV was defined as $2\Delta x/\Delta T$. ΔT is the time for AP propagation from $x-\Delta x$ to $x+\Delta x$. CVR curves were generated by plotting CV against BCL. WL was computed as the product of CV and ERP. VW, which was measured by using a S1-S2 protocol, was an index to quantify the temporal vulnerability of atrial tissue. During the VW, the S2 stimulus can lead to uni-directional conduction block that allows re-entry at the tissue level.

2D simulations

A homogeneous 2D tissue model with 375×375 nodes was developed to investigate spatiotemporal complexity of cardiac dynamics. The membrane potential was computed according to the following equation:

$$\frac{dV}{dt} = -\frac{I_{ion} + I_{stim}}{C_m} + D \cdot \left(\frac{\delta^2 V}{\delta x^2} + \frac{\delta^2 V}{\delta y^2} \right) \quad [11]$$

where the time step (Δt) and the space step (Δx=Δy) are set to be 0.005 ms and 0.1 mm, respectively.

The substrate size, which was measured by using a S1-S2 protocol, was an index to quantify the spatial vulnerability of atrial tissue. In the homogeneous 2D tissue sheet, a planar wave was initiated by a S1 stimulus at the left edge of the sheet. During the VW of this tissue sheet, a S2 stimulus was applied to a center region with the same width (1.0 mm) and different lengths to evoke a conduction wave resulting in a figure-of-eight re-entrant wave. The minimal substrate size was defined as the minimal size of the S2 stimulus necessary to form and sustain reentry. We also simulated spiral waves in the homogeneous 2D tissue sheet using the standard S1-S2 protocol used in a previous study (78). The stability of re-entrant waves was evaluated by computing the path and the area of tip mender. The LS was measured as the time duration in which the spiral wave persists. The dominant frequencies of AP profiles from a fixed site were computed using fast Fourier transform techniques.

3D simulations

A 3D homogeneous human atrium, which was generated by integrating cellular electrical properties into the 3D human anatomical atria geometry, was developed to simulated electrical waves. The membrane potential was computed according to the following equation:

$$\frac{dV}{dt} = -\frac{I_{ion} + I_{stim}}{C_m} + D \cdot \left(\frac{\delta^2 V}{\delta x^2} + \frac{\delta^2 V}{\delta y^2} + \frac{\delta^2 V}{\delta z^2} \right) \quad [12]$$

where the space step (Δx=Δy=Δz) are set to be 0.33 mm. Scroll waves were initiated by using a cross-field protocol similar to that used in the 2D cases.

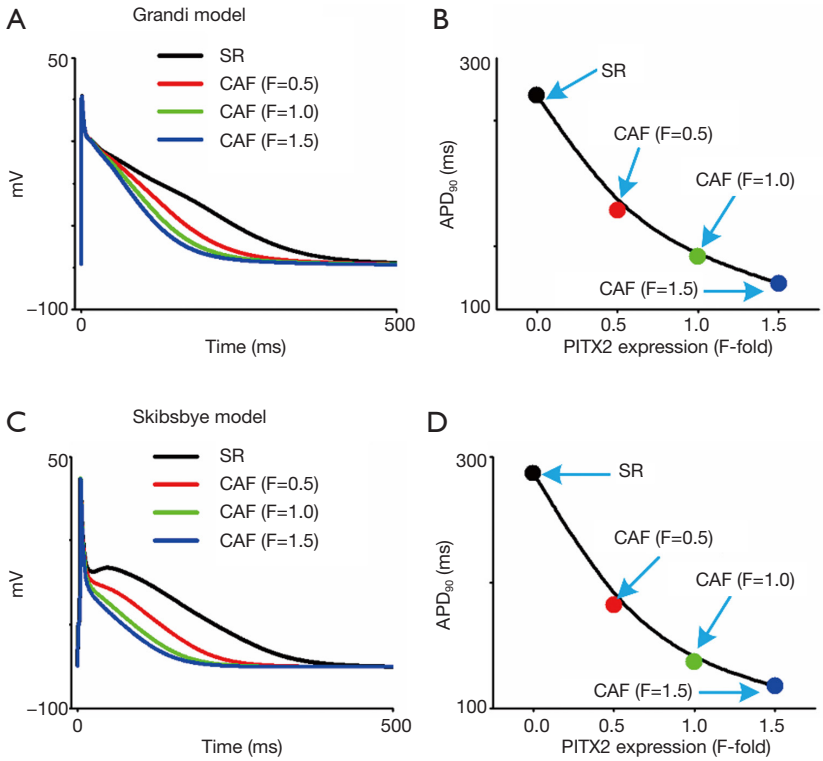

Figure S1 Simulated AP profiles using the human atrial model developed by Grandi *et al.* (Grandi model) and Skibsbye *et al.* (Skibsbye model), as the modelling parameter F is increased from 0 (SR) to 1.5 (CAF) condition. (A,B) AP profiles and APD using the Grandi model; (C,D) AP profiles and computed APD using the Skibsbye model. AP, action potential; SR, sinus rhythm; CAF, chronic atrial fibrillation; APD, AP duration; PITX2, paired-like homeodomain transcription factor 2.

Table S1 Quantitative summary of the effects of PITX2 overexpression on human atrial electrical activity at the single cell level

Model	Quantity	SR (F=0.0)	CAF (F=0.5)	CAF (F=1.0)	CAF (F=1.5)
Grandi model	Resting potential (mV)	−73.19	−73.19	−73.19	−73.19
	APD_{90} (ms)	319.94	228.40	191.98	170.47
	Overshoot (mV)	27.04	27.02	26.99	26.96
	dV/dt_{max} (mV/ms)	213.95	213.91	213.88	213.85
Skibsbye model	Resting potential (mV)	−74.63	−74.63	−74.63	−74.63
	APD_{90} (ms)	286.66	181.97	136.77	117.45
	Overshoot (mV)	37.30	37.17	37.04	36.91
	dV/dt_{max} (mV/ms)	220.71	220.61	220.51	220.40

PITX2, paired-like homeodomain transcription factor 2; SR, sinus rhythm; CAF, chronic atrial fibrillation; APD_{90}, AP repolarization at 90%.